Boletim da Sociedade Astronômica Brasileira, **35**, no. 1, 283-287

The environment of local analogues to high-redshift star forming galaxies

Vitor L. da Silva[1], Thiago S. Gonçalves[1], Arianna Cortesi[1], & Luidhy Santana-Silva[2]

[1] Valongo Observatory - UFRJ e-mail: vitor15@ov.ufrj.br
[2] UNICID

Abstract. High-redshift galaxies form more stars per unit of time compared to galaxies in the local universe. However, it remains unclear whether the trigger for this high star formation rate is related to interactions with the environment or star formation in clumps, due to disk instabilities. The main goal of this project is to investigate the environment of high-redshift analogues, such as Lyman Break Analogues (LBAs), to better understand the influence of the local environment on their properties. Subsequently, these results will be compared with galaxies in the distant universe to evaluate the influence of the local environment on the formation of galaxies 10 billion years ago. Our methodology involves a code that analyzes the fields of the galaxies and measures their respective densities using the k-th nearest neighbor method with $k = 4$, $k = 5$ and $k = 10$. The values of the densities are then compared for different ks. This algorithm was applied to all the galaxies in the DR3 S-PLUS. To evaluate the completeness of our sample, a Schechter function was fitted over the luminosity distribution. The densities were then plotted against galaxy properties to test the robustness of our catalog, and the known relations were successfully recovered.

Resumo. Galáxias de alto redshift formam mais estrelas por unidade de tempo em comparação com galáxias no universo local. No entanto, ainda não temos certeza se o gatilho para essa alta taxa de formação estelar está relacionado à interação com o ambiente ou à formação estelar em *clumps*, devido a instabilidades no disco. O objetivo principal deste projeto é investigar o ambiente de galáxias análogas de alto redshift, como as Análogas de Lyman Break (LBAs), a fim de entender melhor a influência do ambiente local em suas propriedades. Posteriormente, esses resultados serão comparados com galáxias no universo distante para avaliar a influência do ambiente local na formação de galáxias há 10 bilhões de anos. Nossa metodologia envolve um código que analisa os campos das galáxias e mede suas respectivas densidades usando o método dos k-vizinhos mais próximos com $k = 4$, $k = 5$ e $k = 10$. Os valores das densidades são então comparados para diferentes valores de k. Esse algoritmo foi aplicado a todas as galáxias no DR3 S-PLUS. Para avaliar o quão completa nossa amostra é, ajustamos a função de Schechter sobre a distribuição de luminosidades. As densidades foram então plotadas em relação às propriedades das galáxias para testar o quão robusto nossas medidas são, e as relações conhecidas na literatura foram recuperadas com sucesso.

Keywords. Galaxies: evolution – Galaxies: high-redshift – Galaxies: starburst – Galaxies: interactions

1. Introduction

Galaxies in the distant universe form significantly more stars per unit of time compared with galaxies of similar stellar mass values in the local universe Whitaker et al. (2012). In addition, the star formation rate (SFR) density of the universe peaks at around redshift $z \sim 2$, the so-called cosmic noon Madau & Dickinson (2014). However, we don't know whether the main trigger for this high SFR is related to internal processes, such as star formation in clumps due to disk instabilities, or to external processes, such as environmental effects. In order to investigate this possible connection between the environment and the physical properties of those galaxies, we analyze the neighborhood of low-redshift galaxies analogous to typical high-redshift star-forming galaxies (SFGs). The Lyman Break Analogs (LBAs), which are similar to the Lyman Break Galaxies (LBGs, $z \sim 2$) in FUV luminosity ($10.3 \leq \log L_{1530}(L_{\odot}) \leq 10.9$), FUV surface brightness ($9.0 \leq \log I_{1530}\,(L_{\odot}kpc^{-2}) \leq 10.3$), stellar mass ($9.0 \leq \log M_{*}\,(M_{\odot}) \leq 10.7$), star formation rate ($0.5 \leq \log SFR\,(M_{\odot}yr^{-1}) \leq 2$), specific star formation rate ($-9.3 \leq \log SFR/M_{*}\,(yr^{-1}) \leq -8$), FUV attenuation ($0 \leq A_{1530} \leq 2$) and O/H abundance ($8.1 \leq 12 + \log(O/H) \leq 10.9$) Hoopes et al. (2007), constitute an ideal sample for such an investigation.

2. Sample

Our main sample is obtained from the S-PLUS Data Release 3 (Mendes de Oliveira et al. 2019). The S-PLUS survey will observe ≈ 9300 deg^2 of the celestial sphere in 12 bands, 5 broad bands (u, g, r, i and z) and 7 narrow bands (centered on transition lines of spectral features and ISM diagnostics), using a dedicated robotic telescope of 0.8m, the T80-South, at the Cerro Tololo Inter-American Observatory, Chile (Mendes de Oliveira et al. 2019). We also make use of the SeXtractor photometric flags and parameters such as the full width at half maximum (FWHM from here on). To exclude point source objects, we chose only those with a FWHM greater than the seeing of the observations, i.e., `fwhm_n` ≥ 1.5, to select only extended objects. The SeXtractor photometric flags were also used to improve the quality of our sample, with a cut of `photoflag_r` < 3.

In addition to the twelve-band photometry, three Value Added Catalogs (VACs) are available: one with the estimated photometric redshifts (Lima et al. 2022), one with the probability of an object being a galaxy, star or quasar (Nakazono et al. 2021) and one for stellar masks, made to minimize the effect of bright stars. Since the redshift and probability VACs are made with machine learning methods, there are some caveats. Even when accounting only for the objects with a high probability of being a galaxy, we still have some contamination from stars and quasars. To minimize stellar contamination and considering the caveats of each VAC, we selected objects with a probability of being a galaxy greater than or equal to 70% and a stellar mask `flag` $= 0$ (the object is not affected by any star). Measurements for galaxies outside the intervals $14 <$ `r-band` < 21.3 and $0.007 <$ `photo-z` < 0.6 in the training sample are considered extrapolation and should be used with caution. Also, the redshift distribution has a plateau around `photo-z` > 0.4, but

the origin and how this plateau is related with contamination by stellar objects and QSOs is not within the scope of this work, so we consider only the $0.007 <$ `photo-z` < 0.4 interval. The redshift VAC also contains the odds parameter, indicating the quality of the photo-z measure. We consider only objects where `odds` ≥ 0.4.

In short, we applied the following cuts in the DR3 S-PLUS sample:

- `fwhm_n` ≥ 1.5
- `photoflag_r` < 3
- `SNR` > 3
- $14 <$ `r-band` < 21.3
- `PROB_GAL` ≥ 0.7
- $0.007 <$ `photo-z` < 0.4
- `odds` ≥ 0.4
- Stellar Masks: `flag` $= 0$

In total, we have 791 088 objects in our sample.

3. Completeness

To evaluate how complete our sample is we measured the luminosity of all objects using the photometric redshifts, divided the distribution into bins of 0.05dex and fitted a Schechter luminosity function (Schechter 1976) in the r-band luminosity distribution. The Schechter luminosity function is given by:

$$\phi(L_r) = \phi^* \, (\frac{L_r}{L_r^*})^{\alpha} \; exp^{-\frac{L_r}{L_r^*}} \tag{1}$$

where ϕ^* is the normalization factor, L_r^* is the luminosity of the knee and α is the inclination of the low-luminosity side.

Fig. 1 shows the luminosity distribution and the fitted Schechter function for four different redshift intervals. Our estimated model agrees with our data for $log_{10}L_r^*$ above 9.075 for $0.007 < z < 0.1$, 10.075 for $0.1 < z < 0.2$, 10.275 for $0.2 < z < 0.3$ and 10.575 for $0.3 < z < 0.4$ (dashed vertical red lines in Fig. 1). We argue that the disagreement at lower luminosities stems from the incompleteness of our sample at such magnitudes, and thus consider such thresholds (indicated by vertical red dashed lines) as the limits for completeness at each redshift bin.

This is expected because as we go to higher redshifts it's harder to detect the more faint objects. For luminosities below these values, our completeness drops quickly, in a way that we have a bias in our sample for more luminous objects.

4. Methodology

To calculate the density of the environment, we choose the k-th Nearest Neighbor method (KNN method, hereafter). The KNN method consists of choosing an appropriate value for k and evaluate the transversal distance to the k-th nearest neighbor. Galaxies with smaller distances to their neighbor inhabit denser environments; therefore, for a given k, we measure the distance of the galaxy to their neighbor and calculate the projected surface density, defined as:

$$\delta_k = \frac{k}{\pi r_k^2}, \tag{2}$$

where k is the number of neighbors chosen and r_k is the projected distance to the kth nearest neighbor.

The value of k must be taken into account carefully when obtaining the density of the environment (Muldrew et al. 2012). Low values, e.g. $k = 1, 2, 3$, can lead to unrealistic high densities because of clustering of unrelated galaxies and Poisson noise. To probe the immediate surroundings of a galaxy, typical values of $k = 4, 5$ are used, while a typical value of $k = 10$ is used for cluster-scale environments. We compared the results for 3 values of k in this work: $k = 4, 5$ and 10.

Since equation (2) yields the projected density, two galaxies can appear close to each other in the sky, but in reality be very distant to each other along the line-of-sight. To mitigate this projection effect, one generally adopts a redshift slice or a velocity cut. We assume a redshift slice of $\Delta z = 0.015$ for all the galaxies.

When spectroscopic information is available a typical value of $c\Delta z = \pm 500$ km s^{-1}, or $\Delta z \approx \pm 0.0015$, can be used (Muldrew et al. 2012; Gallazzi et al. 2009). For photometric redshifts we can assume that the redshift slice is of the same order of the redshift error, typically being $c\Delta z = \pm 6000$ km s^{-1}, or $\Delta z \approx \pm 0.02$ (Muldrew et al. 2012; Gallazzi et al. 2009).

In order to test for the impact of redshift slice widths in our results, we calculated the $k = 4$ densities for the Stripe 82 region assuming four different values: $\Delta z = \pm 0.005$, $\Delta z = \pm 0.010$, $\Delta z = \pm 0.015$, $\Delta z = \pm 0.020$. These values are close to the Normalized Mean Absolute Deviation, $\sigma_{NMAD} \sim 0.01$ of photo-z's calculated for the galaxies in the DR3 S-PLUS survey (Lima et al. 2022). We determine that $\Delta z = 0.015$, close to the determined NMAD, is ideal; larger values have little impact, while values of 0.01 and smaller severely affect the measured densities due to source exclusion.

We also use the correction function $\psi(z)$ to correct the sample for the Malmquist bias. The correction function $\psi(z)$ is a function of the redshift distribution and follow the relations below:

$$N(z)dz = Az^2\psi(z)dz, \tag{3}$$

where

$$\psi(z) = e^{-\frac{z}{z_c}^{\alpha}}, \tag{4}$$

A is the normalization factor, z_c is a characteristic redshift related to the peak of the redshift distribution, z is the redshift and $N(z)$ is the number of galaxies with redshift measurements between z and $z + dz$. We can see from equations (3) that the number of observed galaxies increase with the redshift as z^2 since we are observing a larger spatial volume, but the observational magnitude limit as described by $\psi(z)$ will hamper our ability to detect faint galaxies at larger redshifts. The best-fit values for our sample are $A = (8 \pm 3) \cdot 10^6$, $z_c = 0.05 \pm 0.02$, $\alpha = 0.8 \pm 0.1$. In order to minimize significant fluctuations and uncertainties in density measurements, we selected galaxies for which $\psi(z) \geq 0.1$, corresponding to $z < 0.14$. With this cut our final sample is composed of 243 370 galaxies.

The projected surface density of a galaxy with respect to their k-th neighbor becomes:

$$\Sigma_k = \frac{k}{\pi r_k^2} \frac{1}{\psi(z)}, \tag{5}$$

where Σ_k is the projected density, r_k^2 is the distance to the k-th neighbor, $\psi(z)$ is the correction function, within a given redshift slice.

5. Results

5.1. Methodology verification

Fig. 2 shows our density map for the Hydra Cluster region, with increased density in the center of the field as expected.

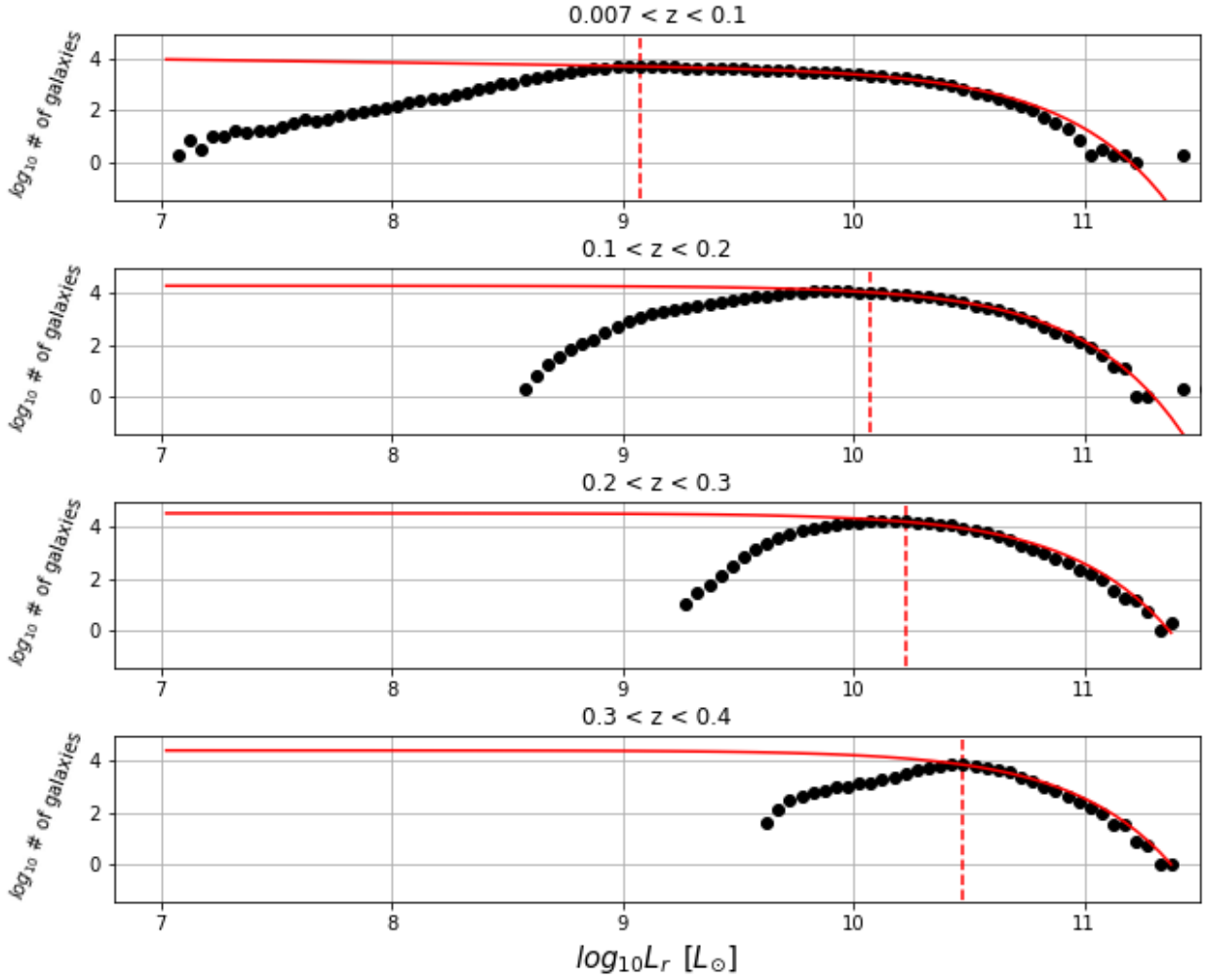

Figure 1. Schechter luminosity function analysis. The black points are the binned luminosity distribution of our S-PLUS DR3 sample. The red solid line is the best fit for Eq. 1 over the data. The red dashed line indicates where our data begins to agree with the model, i.e., where our data have 100% completeness. Our sample is not complete for low luminosity objects, and this bias is stronger with increasing redshift, as we expected.

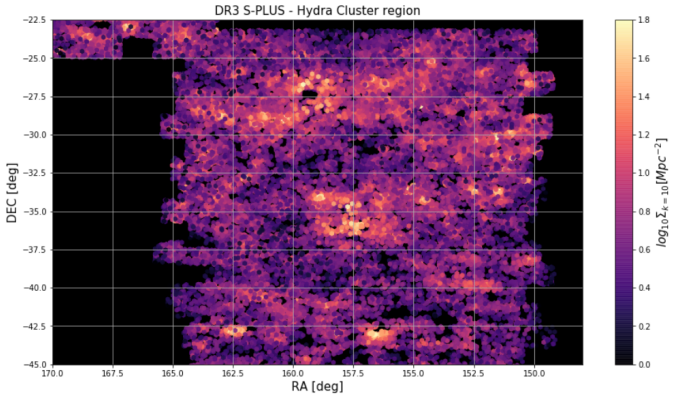

Figure 2. The Hydra Cluster region of the DR3 S-PLUS. The color represents the KNN density for $k = 10$, with brighter points indicating denser environments.

At this stage we intend to verify our methodology and confirm its validity. To do this, we tested how the galaxy properties change as a function of density, as shown in Fig. 3. The top row shows the SFR-, morphology- and mass-density relations. The bottom row present the sSFR-, color- and Age-density relations.

It is clear that galaxies are redder galaxies are found in denser environments, as expected, since red galaxies are more associated with an old star population and no star formation, in contrast with the blue star-forming galaxies, more frequently found in less dense environments. The morphology-density relation, first demonstrated by Oemler (1974) and Dressler (1980), clearly shows that the frequency of late-type galaxies decreases with the environment, while the early-type frequency increases with density. This is in agreement with previous results, meaning that early-type galaxies are more frequently found in denser environments, like cluster cores, while late-type galaxies are found more often in groups and in the field. In a related result, the mass-density relation indicates that more massive objects are found in denser environments.

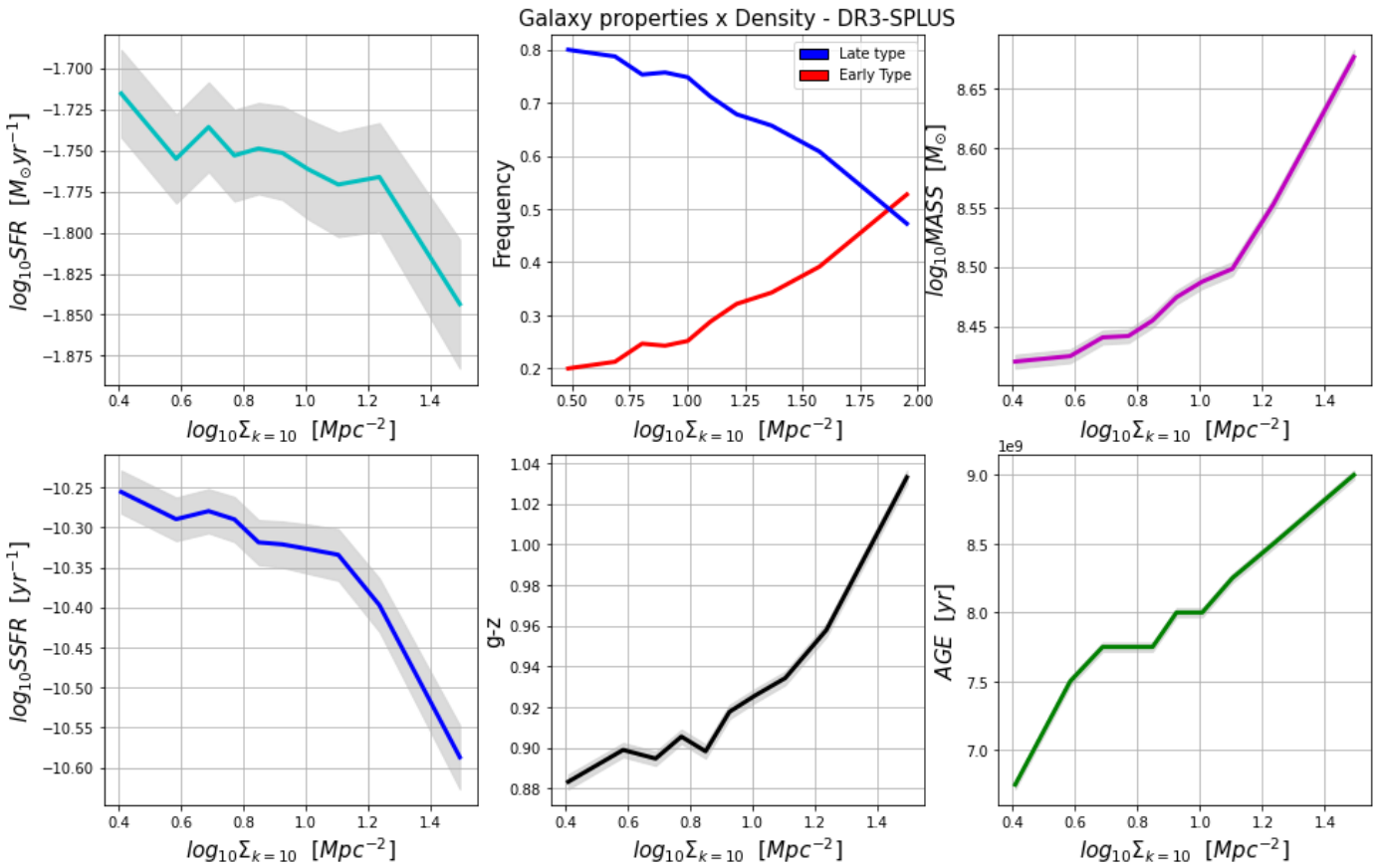

Figure 3. Galaxy properties as a function of environment density. The top row shows the SFR, morphology and mass relations. The bottom row present the sSFR, color and Age relations. The gray shaded regions indicates the errors.

We emphasize that our survey is deep enough to show such trends even with our selection bias toward more massive and luminous galaxies. Since most of the galaxies in the low-density bins are still blue, late-type, and less massive, it is expected that the SFR-density relation should decrease with density, as shown here. Star-forming galaxies are more prevalent in the periphery of clusters and other low-density environments. The $sSFR^{-1}$ value indicates how long a galaxy would take to form its present mass, assuming the present SFR, so it is expected that higher values of sSFR are associated with blue, active star-forming galaxies that typically reside in low-density environments.

5.2. Applications

The aim of this paper is to present a coherent and reliable catalog of densities for the galaxies in the DR3 S-PLUS, i.e. present data for the community. As shown above, one of the utilities for those densities come from comparing how other properties relate with the environment. Bom et al. (2023) measured the probability of a galaxy being late-type or early-type using machine learning, and in one of the tests they used our environment data to successfully reproduce the morphology-density relation.

Another use for our data is the comparison of the densities between different galaxy populations. It is expected that galaxies inhabiting denser environments can experience more mergers than galaxies in low density environments. Santana-Silva et al. (2020) compared the density of Lyman Break Analogs (LBAs, Heckman et al. (2005), Hoopes et al. (2007)) with galaxies of similar mass in the same epochs, and found that these high-redshift analogues are found in higher $k = 4$ densities than the field but similar $k = 10$ densities, indicating that they might inhabit small groups but do not reside in clusters of galaxies.

Finally, one other use for the density map is to locate where galaxy populations are located in the large-scale structure. Smith Castelli et al. (submitted) studied the Hα galaxy population in the Fornax cluster and also presented a brief density analysis of the sample, showing that there are broadly two distinct Hα populations, one composed mainly of late-type galaxies in denser regions and other in peculiar galaxies in the outskirts of the cluster, with the frequency of Hα emitters increasing with decreasing density.

One should notice that our data rely on *photometric redshift estimations*, so the precise characterization of voids and filaments is not clear, since the uncertainty in the line-of-sight can smooth out features in the density map. Another caveat is the bias in our sample for the most luminous objects, in a way that only the more luminous and clustered regions are more precise and complete.

In the near future, we intend to use these results to measure the density of LBAs found within the footprint of S-PLUS. This would complement the work by Santana-Silva et al. (2020) for a much larger sample, considerably improving on the statistics from the previous study.

References

Hoopes, C. G. et al. 2007, The Astrophysical Journal Supplement Series, 173, 441
Mendes de Oliveira, C. et al. 2019, Monthly Notices of the Royal Astronomical Society, 489, 241

Santana-Silva, L. et al. 2020, Monthly Notices of the Royal Astronomical Society, 498, 5183
Whitaker, K. E. et al. 2012, The Astrophysical Journal Letters, 754, L29
Madau P., Dickinson M. 2014, Annual Review of Astronomy and Astrophysics, 52, 415
Lima, E. V. R. et al. 2022, Astronomy and Computing, 38, 100510
Nakazono, L. et al. 2021, Monthly Notices of the Royal Astronomical Society, 507, 5847
Skrutskie, M. F. et al. 2006, The Astronomical Journal, 131, 1163
Lang, D. 2014, The Astronomical Journal, 147, 108
Muldrew, S. I. et al. 2012, Monthly Notices of the Royal Astronomical Society, 419, 2670
Dressler, A. 1980, Astrophysical Journal, 236, 351
Oemler, A. 1974, Astrophysical Journal, 194, 1
Schechter, P. 1976, Astrophysical Journal, 203, 297
Bom, C. R. et al. 2023, Monthly Notices of the Royal Astronomical Society
Gallazzi, A. et al. 2009, Astrophysical Journal, 690, 1883
Santana-Silva, L. et al. 2020, MNRAS, 498, 5183
Hoopes, C. G. et al. 2007, ApJS, 173, 441
Heckman, T. M. et al. 2005, ApJL, 619, L35